

# Enhanced peak growth of global vegetation and its key mechanisms

Kun Huang<sup>1,2</sup>, Jianyang Xia<sup>1,2\*</sup>, Yingping Wang<sup>3,4</sup>, Anders Ahlström<sup>5,6</sup>, Jiquan Chen<sup>7</sup>, Robert B. Cook<sup>8</sup>, Erqian Cui<sup>1,2</sup>, Yuanyuan Fang<sup>9</sup>, Joshua B. Fisher<sup>10</sup>, Deborah Nicole Huntzinger<sup>11</sup>, Zhao Li<sup>1,2</sup>, Anna M. Michalak<sup>9</sup>, Yang Qiao<sup>1,2</sup>, Kevin Schaefer<sup>12</sup>, Christopher Schwalm<sup>13</sup>, Yaxing Wei<sup>14</sup>, Xiaoni Xu<sup>1,2</sup>, Liming Yan<sup>1,2</sup>, Yiqi Luo<sup>15</sup>

<sup>1</sup>Research Center for Global Change and Ecological Forecasting & Tiantong National Forest Ecosystem Observation and Research Station, School of Ecological and Environmental Sciences, East China Normal University, Shanghai 200241, China;

<sup>2</sup>Institute of Eco-Chongming (IEC), 3663 N. Zhongshan Rd., Shanghai 200062, China;

<sup>3</sup>CSIRO Oceans and Atmosphere, PMB 1, Aspendale, Victoria 3195, Australia;

<sup>4</sup>Terrestrial biogeochemistry group, South China Botanic Garden, Chinese Academy of Sciences, Guangzhou, China;

<sup>5</sup>Department of Physical Geography and Ecosystem Science, Lund University, 223 62 Lund, Sweden;

<sup>6</sup>Stanford University, Department of Earth System Science, School of Earth, Energy and Environmental Sciences, 397 Panama Mall, Stanford, CA 94305, USA;

<sup>7</sup>Center for Global Change and Earth Observations and Department of Geography, Environment, and Spatial Sciences, Michigan State University, East Lansing, MI 48824, USA;

<sup>8</sup>Environmental Sciences Division, Oak Ridge National Laboratory, Oak Ridge, TN 37831, USA;

<sup>9</sup>Department of Global Ecology, Carnegie Institution for Science, Stanford, CA 94305, USA;

<sup>10</sup>Jet Propulsion Laboratory, California Institute of Technology, 4800 Oak Grove Drive, Pasadena, CA 91109, USA;

<sup>11</sup>School of Earth Sciences and Environmental Sustainability, Northern Arizona University, Flagstaff, Arizona 86011, USA;

<sup>12</sup>National Snow and Ice Data Center, Cooperative Institute for Research in Environmental Sciences, University of Colorado, Boulder, CO 80309-0449, USA;

<sup>13</sup>Woods Hole Research Center, Falmouth, MA 02540, USA;

<sup>14</sup>Environmental Sciences Division and Climate Change Science Institute, Oak Ridge National Laboratory, Oak Ridge, TN 37831, USA;

<sup>15</sup>Center for ecosystem science and society, Northern Arizona University, Arizona, Flagstaff, AZ 86011, USA;

**Manuscript type:** Article

\*Correspondence to: Jianyang Xia: [jyxia@des.ecnu.edu.cn](mailto:jyxia@des.ecnu.edu.cn)

Manuscript for *Nature Ecology Evolution*

36 *Abstract*

37 **The annual peak growth of vegetation is critical in characterizing capacity of terrestrial**  
38 **ecosystem productivity<sup>1</sup> and shaping the seasonality of the atmospheric CO<sub>2</sub>**  
39 **concentrations<sup>2-5</sup>. The recent greening of global lands<sup>6,7</sup> suggests an increasing trend of**  
40 **terrestrial vegetation growth, but whether the peak growth has been globally enhanced**  
41 **still remains unclear. Here we used two global datasets of gross primary productivity**  
42 **(GPP) and a satellite-derived Normalized Difference Vegetation Index (NDVI) to**  
43 **characterize recent changes in annual peak vegetation growth (i.e., GPP<sub>max</sub> and NDVI<sub>max</sub>).**  
44 **We demonstrated that the peak in growth of global vegetation has been linearly**  
45 **increasing during the past three decades. About 65% of the NDVI<sub>max</sub> variation is near**  
46 **evenly explained by the expanding croplands (21%), rising CO<sub>2</sub> (22%), and intensifying**  
47 **nitrogen deposition (22%). The contribution of expanding croplands to the peak growth**  
48 **trend was substantiated by measurements from eddy-flux towers, sun-induced**  
49 **chlorophyll fluorescence and a global database of plant traits, all of which demonstrated**  
50 **that croplands have a higher photosynthetic capacity than other vegetation types. The**  
51 **large contributions of CO<sub>2</sub> are also supported by a meta-analysis of 466 manipulative**  
52 **experiments and 15 terrestrial biosphere models. Furthermore, we showed that the**  
53 **contribution of GPP<sub>max</sub> to the change in annual GPP is less in tropics than other regions.**  
54 **These findings strengthen the empirical evidence on increasing trends in peak vegetation**  
55 **growth, and highlight the important roles of agricultural intensification and atmospheric**  
56 **changes in reshaping the seasonality of global vegetation growth.**

57 **Main**

58 The temporal dynamics of atmospheric CO<sub>2</sub> concentrations ([CO<sub>2</sub>]) are inversely correlated  
59 with that of terrestrial CO<sub>2</sub> uptake and vegetation growth<sup>4,8</sup>. Atmospheric monitoring has  
60 revealed an increase of 30 to 60% in the seasonal amplitude of CO<sub>2</sub> concentrations over the  
61 Northern Hemisphere since the 1960s<sup>4,8-12</sup>. The enhanced seasonal CO<sub>2</sub> amplitude is largely  
62 driven by the increasing drawdown of the trough of the CO<sub>2</sub> seasonal cycle in the Northern  
63 Hemisphere during summer, when CO<sub>2</sub> uptake resulting from vegetation growth also peaks.  
64 Recent evidence has also shown that the inter-annual variation of terrestrial net C uptake  
65 correlates more strongly with the peak gross primary productivity (GPP) than any climatic  
66 factors<sup>1,13,14</sup>. In addition, global lands have been greening since 1980s<sup>6,7</sup>. All these lines of  
67 evidence imply an increasing peak growth of vegetation, but whether such trend exists globally  
68 or mainly in some specific regions remains unknown. A continuing increase of peak vegetation  
69 growth is ecologically possible, because measurements of modern-plant traits have found large  
70 variations in leaf photosynthetic capacity among/within plant functional types<sup>15</sup> and  
71 palaeoecological studies have revealed a highly flexibility of maximum individual size of  
72 vascular plants under different climatic regimes<sup>16</sup>. Thus, to better predict the temporal trends  
73 of land sink capacity and atmospheric [CO<sub>2</sub>] dynamics, we need to examine whether the peak  
74 growth of global vegetation has been enhanced in the past years, and to understand the global  
75 distributions of the change in peak vegetation growth and their driving factors.

76 Here, we examined the trends of peak vegetation growth using two proxies [i.e., maximal  
77 monthly GPP (GPP<sub>max</sub>) and maximal monthly Normalized Difference Vegetation Index  
78 (NDVI<sub>max</sub>)] and identified their key driving factors. The global-scale GPP datasets were  
79 derived by a machine learning technique known as model tree ensemble (MTE) with  
80 FLUXNET measurements<sup>17</sup>. The NDVI data was obtained from Global Inventory Modeling  
81 and Mapping Studies (GIMMS) that has been corrected for satellite sensor drift<sup>18</sup>. We  
82 investigated the difference in photosynthetic capacity among plant functional types using  
83 measurements of sun-induced chlorophyll fluorescence (SIF) from the Global Ozone  
84 Monitoring Experiment 2 (GOME-2)<sup>19</sup>, flux tower measurements from FLUXNET<sup>1</sup>, and plant

85 functional traits from TRY database<sup>15</sup> (see Methods). A meta-analysis of 466 experiments  
86 (Supplementary Table 2) was further conducted to compare the contributions of elevated CO<sub>2</sub>,  
87 climate warming, and nitrogen addition to peak accumulation of plant biomass (see Methods).  
88 Finally, using modelling results from the Multi-scale Synthesis and Terrestrial Model  
89 Intercomparison Project (MsTMIP) project<sup>20</sup> (see Methods), we quantified the contributions of  
90 changes in land cover, climate and atmosphere to the simulated trends of global peak GPP.

91 The two indices of peak vegetation growth across the globe consistently show linearly  
92 increasing trends during the past three decades (1982-2011 for MTE GPP and NDVI), with the  
93 global trends of MTE GPP<sub>max</sub> and NDVI<sub>max</sub> as 3.931 g C m<sup>-2</sup> yr<sup>-2</sup> ( $P < 0.05$ ) and 0.0013 yr<sup>-1</sup> ( $P$   
94  $< 0.05$ ), respectively (Fig. 1). The observed increase in global averaged MTE GPP<sub>max</sub> was  
95 consistent with the observed growth in atmospheric CO<sub>2</sub> amplitude at Point Barrow (BRW:  
96 71.3°N, 156.6°W;  $r^2=0.32$ ,  $P<0.01$ ) (Supplementary Fig. 1). Globally, the fastest increase in  
97 peak vegetation-growth occurred in areas of intense agricultural activities, such as Northern  
98 China, India, Western Europe and North America (Fig. 1b and c; Supplementary Fig. 2).  
99 Additionally, the monthly maximal enhanced vegetation index (EVI<sub>max</sub>) illustrated similar  
100 patterns of increasing trends globally over 2000-2011 (Supplementary Fig. 3).

101 We then applied a relative importance algorithm (see Methods) to attribute the annual  
102 changes in NDVI<sub>max</sub> during 1982-2010 to its drivers. (Note that we did not attribute MTE  
103 GPP<sub>max</sub>, because climate and land use data were used as explanatory variables to train MTE  
104 GPP.) The driving factors included solar radiation (Rad), air temperature (Tmp), precipitation  
105 (Pre), agricultural activities (i.e., fractional change of cropland; Agr), rising CO<sub>2</sub> (CO<sub>2</sub>), and  
106 nitrogen deposition (NDE). The contribution of each factor was calculated for each grid cell  
107 (Supplementary Fig. 4), and the factor that made the greatest contribution to the NDVI<sub>max</sub>  
108 variation was identified as the dominant driver (Fig. 2a). At the global scale, around 65% of  
109 NDVI<sub>max</sub> variation could be explained by the combination of changes in atmospheric [CO<sub>2</sub>]  
110 (22%), the rate of nitrogen deposition (22%), and cropland fraction (21%) (Fig.2a). These three  
111 factors were also the primary explanatory factors along the global latitudinal gradient (Fig. 2b).  
112 Although croplands only accounted for around 13.8% of the land area globally (Supplementary

113 Fig. 5a), it contributed to 31.8% of the global increasing  $GPP_{max}$  trends (Supplementary Fig.  
114 5b). Also, higher intra-biome fractions of significant  $GPP_{max}$  trends were found in croplands  
115 than other biomes (Supplementary Fig. 5c).

116 The large contribution of agricultural activities appeared to be caused by the higher  
117 photosynthetic capacity that crops have over non-crops species. Here we analyzed observed  
118 multi-levels photosynthetic capacity data in three biome groups: cropland (CRO), forest (FOR),  
119 grassland (GRA), respectively. Leaf-level maximum carboxylation rate (i.e.,  $V_{cmax}$ ) from 612  
120 observations<sup>21-23</sup> across 81 species showed that crops ( $85.2 \pm 31.0 \mu\text{mol m}^{-2} \text{s}^{-1}$ ) have larger  
121  $V_{cmax}$  than trees ( $56.4 \pm 26.7 \mu\text{mol m}^{-2} \text{s}^{-1}$ ) and grasses ( $36.9 \pm 27.9 \mu\text{mol m}^{-2} \text{s}^{-1}$ ) (Fig. 3a).  
122 Ecosystem-level measurements of daily GPP across 213 eddy-flux sites also demonstrated the  
123 higher  $GPP_{max}$  in cropland ( $14.2 \pm 5.7 \text{g C m}^{-2} \text{d}^{-1}$ ) than forest ( $9.7 \pm 3.3 \text{g C m}^{-2} \text{d}^{-1}$ ) and grassland  
124 ( $3.4 \pm 2.3 \text{g C m}^{-2} \text{d}^{-1}$ ) (Fig. 3b). At the biome level, monthly maximal SIF ( $SIF_{max}$ ), retrieved  
125 from GOME-2 spectral instrument (Fig. 3c), showed that croplands ( $1.6 \pm 0.4 \text{mW}^{-1} \text{m}^{-2} \text{sr}^{-1}$   
126  $\text{nm}^{-1}$ ) have a higher maximal photosynthetic capacity than areas of forest ( $1.3 \pm 0.5 \text{mW}^{-1} \text{m}^{-2}$   
127  $\text{sr}^{-1} \text{nm}^{-1}$ ) and grassland ( $1.2 \pm 0.5 \text{mW}^{-1} \text{m}^{-2} \text{sr}^{-1} \text{nm}^{-1}$ ). These findings are consistent with  
128 previous studies that detected higher maximal photosynthetic capacity in croplands than  
129 surrounding dense forests under similar climate conditions<sup>19,24</sup>.

130 The higher contributions of atmospheric  $[\text{CO}_2]$  and nitrogen deposition, compared with  
131 climate warming, stem from two causes. First, as shown by the meta-analysis of 466  
132 experiments across 719 plant species (Supplementary Fig. 6), peak accumulation of leaf  
133 biomass was significantly enhanced by elevated  $\text{CO}_2$  (95% CI of 16.7-24.1%) and nitrogen  
134 addition (12.4-18.5%), and to a lesser extent also by warming (2.3-13.6%) (Fig. 3d). These  
135 results are consistent with the reported, strong, worldwide  $\text{CO}_2$  fertilization effect<sup>25-27</sup> and  
136 nitrogen limitation<sup>28,29</sup> on plant photosynthesis. Second, climate warming benefits plant growth  
137 primarily through advancing spring leaf onset<sup>30</sup>, but could suppress plant peak growth by  
138 triggering summer water deficiency in dry years or regions<sup>31,32</sup>. Warming could also affect  
139 plant growth by increasing soil nitrogen mineralization and availability<sup>33</sup>. In addition, the  
140 effects of elevated  $\text{CO}_2$  and nitrogen addition on plant biomass were significant in almost all

141 plant functional types, whereas the warming effect was insignificant for herbs (Supplementary  
142 Fig. 7). However, it should be noted that croplands are highly managed by humans, so the  
143 difference in environmental contributions in cropland regions is uncertain.

144 We further examined the temporal trend of  $GPP_{max}$  over 1982–2010 from 15 terrestrial  
145 biosphere models (TBMs) from MsTMIP<sup>34</sup>, and evaluated the ability of those models to project  
146 response of  $GPP_{max}$  to climate change (varying temperature, precipitation and radiation), land  
147 use and land cover change (LULCC), rising  $CO_2$ , and nitrogen deposition (Supplementary  
148 Fig.8-11). Globally,  $CO_2$  fertilization and climate change were attributed as primary drivers of  
149 modeled  $GPP_{max}$  trend (Fig.4), although models disagreed on the relative importance of those  
150 two drivers (Table 1). It is noted that the influences of nitrogen deposition might be uncertain  
151 since only a few models (eight out of fifteen) in the ensemble incorporating nitrogen limitation.  
152 Here, when using the models to perform factorial simulations that include nitrogen deposition,  
153 rising  $CO_2$  accounted for  $62 \pm 22\%$  ( $6.12 \pm 2.28 \text{ g C m}^{-2} \text{ yr}^{-2}$ ) of the modeled  $GPP_{max}$  trend  
154 globally, followed by climate change (CLI;  $43 \pm 14\%$ ,  $4.32 \pm 1.32 \text{ g C m}^{-2} \text{ yr}^{-2}$ ), nitrogen  
155 deposition (NDE;  $1 \pm 8\%$ ,  $0.12 \pm 0.72 \text{ g C m}^{-2} \text{ yr}^{-2}$ ) and LULCC ( $-6 \pm 5\%$ ,  $-0.6 \pm 0.48 \text{ g C m}^{-2}$   
156  $\text{yr}^{-2}$ ) (Fig.4a; + Nitrogen). In comparison with models considering carbon-nitrogen (C-N)  
157 cycles, models without C-N couplings demonstrated similar contributions of rising  $CO_2$  and  
158 climate but positive contributions of LULCC to modeled  $GPP_{max}$  trend:  $CO_2$  ( $55 \pm 8\%$ ,  $6 \pm$   
159  $0.84 \text{ g C m}^{-2} \text{ yr}^{-2}$ ), CLI ( $37 \pm 6\%$ ,  $3.96 \pm 0.6 \text{ g C m}^{-2} \text{ yr}^{-2}$ ) and LULCC ( $8 \pm 4\%$ ,  $0.84 \pm 0.48 \text{ g}$   
160  $\text{C m}^{-2} \text{ yr}^{-2}$ ). Compared with the correlations of MTE  $GPP_{max}$  with cropland fractions, the  
161 LULCC effect was underestimated globally (Fig.5a). The LULCC effect might not be  
162 adequately captured by the MsTMIP models since most models do not explicitly represent  
163 crops or agricultural management<sup>35</sup>. Similarly,  $CO_2$  fertilization and climate change effects  
164 were the main drivers of the modeled  $GPP_{max}$  trends in the three latitude zones (northern high-  
165 latitudes, mid-latitudes and tropics), and  $CO_2$  fertilization showed largest contributions ( $70 \pm$   
166  $28\%$ ) to the tropical  $GPP_{max}$  trend (Fig.4b-d). Examining the correlations of MTE  $GPP_{max}$  with  
167 cropland fractional changes (Supplementary Fig.12), modeled LULCC effects were  
168 consistently underestimated in all the latitude zones (Fig.4b-d). The LULCC schemes of  
169 models participating in the MsTMIP varied greatly among models<sup>35</sup>, and differences remained

170 in the model processes relating to the land use change fraction, including the cropland  
171 conversion. The underestimated LULCC effect could also be due to the fact that agricultural  
172 management represented by these models differed significantly by the algorithms specified for  
173 the major crop types, such as fertilizer applications, irrigation or tillage practices<sup>36</sup>.

174 Our study confirms the long-term increase in global vegetation's peak growth during the  
175 past three decades. While there is no single driver for the increase in peak vegetation-growth,  
176 the intensification of agriculture<sup>24,37</sup> and rapid increases in atmospheric [CO<sub>2</sub>]<sup>6,38</sup> and nitrogen  
177 deposition<sup>29,39</sup> have served as the most important forcing factors. The expansion of cropland is  
178 an important driver, because the enhanced GPP<sub>max</sub> and NDVI<sub>max</sub> (Fig. 1b, c) are largely located  
179 in the regions with increasing cropland fractions (Supplementary Fig.12). In those regions with  
180 decreasing cropland fractions, e.g., the Eastern US and Western Europe (Supplementary  
181 Fig.13), no significantly increasing trends of GPP<sub>max</sub> and NDVI<sub>max</sub> were detected (Fig. 1b, c).  
182 The cropland expansion also drives the enhanced NDVI<sub>max</sub> in many tropical regions, partially  
183 because their peak vegetation-growth is not sensitive to the changes in other factors. For  
184 example, the peak growth occurs in dry seasons in many tropical forests with high annual  
185 precipitation<sup>40</sup>. The higher peak growth of crops compared to non-crops plants results from not  
186 only their larger photosynthetic capacity from leaf to community levels (Fig. 3a-c), but also  
187 from the intense management (irrigation and fertilization)<sup>41,42</sup> in croplands during the growing  
188 season<sup>43</sup>, which creates nearly ideal growing conditions that are rare in unmanaged ecosystems.  
189 Rising CO<sub>2</sub> largely controls the trends of peak vegetation growth in both satellite-based and  
190 modeling analyses. It supports the recent finding of a linear relationship between GPP  
191 responses and seasonal atmospheric CO<sub>2</sub> amplitude in reaction to rising CO<sub>2</sub><sup>38</sup>. The dominant  
192 role of rising CO<sub>2</sub> rather than other factors in eastern US and western Europe has also been  
193 reported by the analysis on long-term eddy-flux observations<sup>44</sup>. Because nitrogen is a key factor  
194 determining plant photosynthetic capacity<sup>28,29</sup>, the large contribution of nitrogen deposition to  
195 the enhanced peak growth of vegetation is likely related to plant photosynthetic capacity  
196 stimulated by leaf nitrogen concentrations<sup>45</sup>.

197 A large uncertainty in terrestrial productivity simulated by terrestrial biosphere models

198 has been repeatedly documented over the past few decades<sup>2,46</sup>. This study proposes feasible  
199 improvements to ecosystem productivity simulations in terms of peak vegetation growth. First,  
200 models differed in design of crop types and the ways how these models deal with crop and  
201 agricultural management. MsTMIP models might underestimate the contribution of  
202 agricultural activities to the global increase in vegetation-growth peak, because most models  
203 do not explicitly represent crops and agricultural management<sup>35</sup>. The findings presented here  
204 call for an explicit incorporation of agricultural management—such as planting dates and  
205 harvesting strategies, cultivar choices, as well as fertilizer application and irrigation/tillage  
206 practices—in global C-cycle models<sup>47-50</sup>. Second, further model evaluation and improvement  
207 on the control of leaf nitrogen concentrations and environmental variables (e.g., temperature,  
208 radiation, day length and humidity) on modeling plant photosynthetic capacity (e.g.,  $V_{cmax}$ ) are  
209 needed, as they are conventionally assumed to be constant for each plant functional type or to  
210 vary linearly with leaf nitrogen concentrations in current TBMs<sup>45</sup>.

211 It should be noted that  $GPP_{max}$  contributed less to the temporal changes in annual GPP in  
212 tropics than other regions (Fig.5a), suggesting that the enhanced peak growth does not  
213 necessarily lead to an increase of annual total GPP at the global scale. In fact, observation-  
214 based data sets have shown near-zero or only small increasing trend of global annual GPP  
215 during the past three decades<sup>7,51</sup> (Supplementary Fig.14). However, the efficiency of  
216 productivity (i.e., the NPP/GPP ratio) increases with cropland expansion, rising atmospheric  
217  $[CO_2]$  and enhanced N deposition (Fig. 5b). Thus, more research efforts are still needed to  
218 explore the long-term trend of global NPP, which has been recognized as a measurable  
219 planetary boundary for the biosphere<sup>52</sup>.

220 The global data sets and attribution methods used here have their own uncertainties.  
221 Previous studies have revealed MTE GPP products are partly parameter- and climate-  
222 dependent (i.e., fraction of absorbed photosynthetically active radiation, light use efficiency  
223 and temperature). Thus, study on peak growth of global vegetation could be improved when  
224 independent estimations for global GPP using SIF<sup>53</sup> and/or carbonyl sulfide<sup>54</sup> become available  
225 as global GPP tracers in the future. The Lindeman-Merenda-Gold (LMG) method of relative

226 importance calculation algorithm allows us to differentiate the contributions of correlated  
227 regressors without considering regressors' order effects in a multiple linear regression<sup>55</sup> and  
228 has been widely used to the attributions of observation-based datasets to global environmental  
229 change factors<sup>14,56</sup>, but caution should be taken when evaluating the model factorial  
230 experimental results.

231 Overall, this study has found that increasing trends exist globally and regionally for both  
232 NDVI<sub>max</sub> and GPP<sub>max</sub>. The findings of this study have several important implications. First, our  
233 results suggest that the recent increase of global peak vegetation growth is not only driven by  
234 rising CO<sub>2</sub> and nitrogen deposition but also by agricultural intensification. Second, soil carbon  
235 losses<sup>57</sup> caused by croplands expansion need to be considered in the prediction of future  
236 terrestrial carbon sink under the increasing peak plant growth. Lastly, the projections of future  
237 atmospheric [CO<sub>2</sub>] seasonality would benefit from a better understanding of the processes  
238 regulating peak vegetation growth, such as the seasonal dynamics of leaf photosynthetic  
239 capacity ( $V_{cmax}$ )<sup>58-60</sup>, deforestation<sup>24</sup>, fire<sup>43</sup>, and nutrient limitations<sup>61</sup>.

## 240 **References**

- 241 1. Xia, J. *et al.* Joint control of terrestrial gross primary productivity by plant phenology and  
242 physiology. *Proc. Natl Acad. Sci. USA* **112**, 2788-2793 (2015).
- 243 2. Ahlström, A. *et al.* The dominant role of semi-arid ecosystems in the trend and variability  
244 of the land CO<sub>2</sub> sink. *Science* **348**, 895-899 (2015).
- 245 3. Forkel, M. *et al.* Enhanced seasonal CO<sub>2</sub> exchange caused by amplified plant productivity  
246 in northern ecosystems. *Science* **351**, 696-699 (2016).
- 247 4. Graven, H. D. *et al.* Enhanced Seasonal Exchange of CO<sub>2</sub> by Northern Ecosystems Since  
248 1960. *Science* **341**, 1085-1089 (2013).
- 249 5. Randerson, J. T., Thompson, M. V., Conway, T. J., Fung, I. Y. & Field, C. B. The  
250 contribution of terrestrial sources and sinks to trends in the seasonal cycle of atmospheric  
251 carbon dioxide. *Glob. Biogeochem. Cycles* **11**, 535-560 (1997).
- 252 6. Zhu, Z *et al.* Greening of the Earth and its drivers. *Nat. Clim. Change* **6**, 791-795 (2016).
- 253 7. Anav A, et al. Spatiotemporal patterns of terrestrial gross primary production: A review.

254        *Reviews of Geophysics* **53**, 2015RG000483 (2015).

255 8. Keeling, C. D., Chin J. F. S. & Whorf T. P. Increased activity of northern vegetation  
256 inferred from atmospheric CO<sub>2</sub> measurements. *Nature* **382**, 146-149 (1996).

257 9. Myneni, R. B., Keeling, C. D., Tucker, C. J., Asrar, G. & Nemani, R. R. Increased plant  
258 growth in the northern high latitudes from 1981 to 1991. *Nature* **386**, 698-702 (1997).

259 10. Lucht, W. *et al.* Climatic control of the high-latitude vegetation greening trend and  
260 Pinatubo effect. *Science* **296**, 698-702 (1997).

261 11. Nemani, R. R. *et al.* Climate-driven increases in global terrestrial net primary production  
262 from 1982 to 1999. *Science* **300**, 1560-1563 (2003).

263 12. Xu, L. *et al.* Temperature and vegetation seasonality diminishment over northern lands.  
264 *Nature Clim. Change* **3**, 581-586 (2013).

265 13. Zhou, S. *et al.* Explaining inter-annual variability of gross primary productivity from  
266 plant phenology and physiology. *Agric. For. Meteorol.* **226**, 246-256 (2016).

267 14. Musavi, T. *et al.* Stand age and species richness dampen interannual variation of  
268 ecosystem-level photosynthetic capacity. *Nat. Ecol. Evol.* **1**, 0048 (2017).

269 15. Kattge, J. *et al.* TRY – a global database of plant traits. *Glob. Change Biol.* **17**, 2905-  
270 2935 (2011).

271 16. Stein, W. E., Mannolini F., Hernick L. V., Landing E. & Berry C. M. Giant cladoxylopid  
272 trees resolve the enigma of the Earth's earliest forest stumps at Gilboa. *Nature* **446**, 904-  
273 907 (2007).

274 17. Jung, M. *et al.* Global patterns of land-atmosphere fluxes of carbon dioxide, latent heat,  
275 and sensible heat derived from eddy covariance, satellite, and meteorological  
276 observations. *J. Geophys. Res. Biogeosci.* **116**, G00J07 (2011).

277 18. Hickler, T. *et al.* Precipitation controls Sahel greening trend. *Geophys. Res. Lett.* **32**,  
278 L21415 (2005).

279 19. Guanter, L. *et al.* Global and time-resolved monitoring of crop photosynthesis with  
280 chlorophyll fluorescence. *Proc. Natl Acad. Sci. USA* **111**, 1327-1333 (2014).

281 20. Huntzinger, D. N. *et al.* The North American Carbon Program Multi-Scale Synthesis and  
282 Terrestrial Model Intercomparison Project – Part 1: Overview and experimental design.  
283 *Geosci. Model Dev.* **6**, 2121-2133 (2013).

- 284 21. Medlyn, B. E. et al. Effects of elevated [CO<sub>2</sub>] on photosynthesis in European forest  
285 species: a meta-analysis of model parameters. *Plant Cell & Environment* **22**, 1475-1495  
286 (1999).
- 287 22. Montgomery, R. A. & Givnish T. J. Adaptive radiation of photosynthetic physiology in  
288 the Hawaiian lobeliads: dynamic photosynthetic responses. *Oecologia* **155**, 455-467  
289 (2008).
- 290 23. Wilson, K. B., Baldocchi D. D. & Hanson P. J. Spatial and seasonal variability of  
291 photosynthetic parameters and their relationship to leaf nitrogen in a deciduous forest.  
292 *Tree Physiol.* **20**, 565-578 (2000).
- 293 24. Zeng, N. et al. Agricultural Green Revolution as a driver of increasing atmospheric CO<sub>2</sub>  
294 seasonal amplitude. *Nature* **515**, 394-397 (2014).
- 295 25. Schimel, D., Stephens, B. B. & Fisher, J. B. Effect of increasing CO<sub>2</sub> on the terrestrial  
296 carbon cycle. *Proc. Natl Acad. Sci. USA* **112**, 436-441 (2015).
- 297 26. Ainsworth, E. A. & Long, S. P. What have we learned from 15 years of free-air CO<sub>2</sub>  
298 enrichment (FACE)? A meta-analytic review of the responses of photosynthesis, canopy.  
299 *New Phytol.* **165**, 351-371 (2005).
- 300 27. Luo, Y. Q., Hui, D. F. & Zhang, D. Q. Elevated CO<sub>2</sub> stimulates net accumulations of  
301 carbon and nitrogen in land ecosystems: A meta-analysis. *Ecology* **87**, 53-63 (2006).
- 302 28. LeBauer, D. S. & Treseder, K. K. Nitrogen limitation of net primary productivity in  
303 terrestrial ecosystems is globally distributed. *Ecology* **89**, 371-379 (2008).
- 304 29. Xia, J. Y. & Wan, S. Q. Global response patterns of terrestrial plant species to nitrogen  
305 addition. *New Phytol.* **179**, 428-439 (2008).
- 306 30. Piao, S. et al. Leaf onset in the northern hemisphere triggered by daytime temperature.  
307 *Nat. Commun.* **6**, 6911 (2015).
- 308 31. Niu, S. L. et al. Water-mediated responses of ecosystem carbon fluxes to climatic change  
309 in a temperate steppe. *New Phytol.* **177**, 209-219 (2008).
- 310 32. Xia, J. Y., Niu S. L. & Wan S. Q. Response of ecosystem carbon exchange to warming  
311 and nitrogen addition during two hydrologically contrasting growing seasons in a  
312 temperate steppe. *Glob. Change Biol.* **15**, 1544-1556 (2009).
- 313 33. Rustad, L. et al. A meta-analysis of the response of soil respiration, net nitrogen

- 314 mineralization and aboveground plant growth to experimental ecosystem warming.  
315 *Oecologia*. **126**, 543-562 (2001).
- 316 34. Huntzinger, D.N. *et al.* NACP MsTMIP: Global 0.5-deg Terrestrial Biosphere Model  
317 Outputs (version 1) in Standard Format. ORNL DAAC, Oak Ridge, Tennessee, USA.  
318 <http://doi.org/10.3334/ORNLDAAC/1225> (2016).
- 319 35. Thomas, R.T. *et al.* Increased light-use efficiency in northern terrestrial ecosystems  
320 indicated by CO<sub>2</sub> and greening observations. *Geophys. Res. Lett.* **43**, 11339-11349 (2016).
- 321 36. Wei, Y. *et al.* The North American Carbon Program Multi-scale Synthesis and Terrestrial  
322 Model Intercomparison Project-Part2:Environmental driver data. *Geosci. Model Dev.* **7**,  
323 2875-2893 (2014).
- 324 37. Gray, J. M. *et al.* Direct human influence on atmospheric CO<sub>2</sub> seasonality from increased  
325 cropland productivity. *Nature* **515**, 398-401 (2014).
- 326 38. Wenzel, S., Cox, P. M., Eyring, V. & Friedlingstein, P. Projected land photosynthesis  
327 constrained by changes in the seasonal cycle of atmospheric CO<sub>2</sub>. *Nature* **538**, 499-501  
328 (2016).
- 329 39. Magnani, F. *et al.* The human footprint in the carbon cycle of temperate and boreal forests.  
330 *Nature* **447**, 849-851 (2007).
- 331 40. Guan, K. *et al.* Photosynthetic seasonality of global tropical forests constrained by  
332 hydroclimate. *Nat. Geosci.* **8**, 284-289 (2015).
- 333 41. Sacks, W. J., Cook B. I., Buening N., Levis S. & Helkowski J. H. Effects of global  
334 irrigation on the near-surface climate. *Clim. Dyn.* **33**, 159-175 (2009).
- 335 42. Zhang, X. *et al.* Managing nitrogen for sustainable development. *Nature* **528**, 51-59  
336 (2015).
- 337 43. Zhao, F. *et al.* Role of CO<sub>2</sub>, climate and land use in regulating the seasonal amplitude  
338 increase of carbon fluxes in terrestrial ecosystems: a multimodel analysis.  
339 *Biogeosciences* **13**, 5121-5137 (2016).
- 340 44. Fernández-Martínez, M. *et al.* Atmospheric deposition, CO<sub>2</sub>, and change in the land  
341 carbon sink. *Scientific Reports* **7**, 9632 (2017).
- 342 45. Ali, A. A. *et al.* Global-scale environmental control of plant photosynthetic capacity. *Ecol.*  
343 *Appl.* **25**, 2349-2365 (2015).

- 344 46. Sitch, S. *et al.* Evaluation of the terrestrial carbon cycle, future plant geography and  
345 climate-carbon cycle feedbacks using five Dynamic Global Vegetation Models  
346 (DGVMs). *Glob. Change Biol.* **14**, 2015-2039 (2008).
- 347 47. Bondeau, A. *et al.* Modelling the role of agriculture for the 20th century global terrestrial  
348 carbon balance. *Glob. Change Biol.* **13**, 679-706 (2007).
- 349 48. Gervois, S. *et al.* Including Croplands in a Global Biosphere Model: Methodology and  
350 Evaluation at Specific Sites. *Earth Interactions* **8**, 1-25 (2004).
- 351 49. Han, J., Chen J., Miao Y. & Wan S. Multiple resource use efficiency (mRUE): A new  
352 concept for ecosystem production. *Scientific Reports* **6**, 37453 (2016).
- 353 50. Lawrence, D. M. *et al.* The Land Use Model Intercomparison Project (LUMIP)  
354 contribution to CMIP6: rationale and experimental design. *Geosci. Model Dev.* **9**, 2973-  
355 2998 (2016).
- 356 51. Chen, M. *et al.* Regional contribution to variability and trends of global gross primary  
357 productivity. *Environ. Res. Lett.* **12**, 105005 (2016).
- 358 52. Running, S.W. A measurable planetary boundary for the biosphere. *Science* **337**, 1458-  
359 1459 (2012).
- 360 53. Sun, Y. *et al.* OCO-2 advances photosynthesis observation from space via solar induced  
361 chlorophyll fluorescence. *Science* **358**, doi: 10.1126/science.aam5747 (2017).
- 362 54. Hilton, T.W. *et al.* Peak growing season gross uptake of carbon in North America is  
363 largest in the Midwest USA. *Nat. Clim. Change* **7**, 450-454 (2017).
- 364 55. Yao, Y. *et al.* Spatiotemporal pattern of gross primary productivity and its covariation  
365 with climate in China over the last thirty years. *Glob. Change Biol.* **24**, 184-196 (2018).
- 366 56. Carvalhais, N. *et al.* Global covariation of carbon turnover times with climate in  
367 terrestrial ecosystems. *Nature* **514**, 213-217 (2014).
- 368 57. Sanderman, J., Hengl, T., Fiske, G.J. Soil carbon debt of 12,000 years of human land use.  
369 *Proc Natl Acad. Sci. USA* **114**, 9575-9580 (2017).
- 370 58. Croft, H., Chen, J.M., Luo, X., Bartlett, P., Chen, B., Staebler, R. M. Leaf chlorophyll  
371 content as a proxy for leaf photosynthetic capacity. *Glob. Change Biol.* **23**, 3513-3524  
372 (2017).
- 373 59. Luo, X. *et al.* Incorporating leaf chlorophyll content into a two-leaf terrestrial biosphere

- 374 model for estimating carbon and water fluxes at a forest site. *Agric. For. Meteorol.* **248**,  
375 156-168 (2018).
- 376 60. Alton, P. B. Retrieval of seasonal Rubisco-limited photosynthetic capacity at global  
377 FLUXNET sites from hyperspectral satellite remote sensing: Impact on carbon modelling.  
378 *Agric. For. Meteorol.* **232**, 74-88 (2017).
- 379 61. Wieder, W. R., Cleveland, C. C., Smith, W. K. & Todd-Brown, K. Future productivity  
380 and carbon storage limited by terrestrial nutrient availability. *Nat. Geosci.* **8**, 441-444  
381 (2015).

## 382 **Methods**

383 **Flux tower-based and satellite GPP data:** We included 30-year eddy covariance flux-based  
384 and 15-year MODIS satellite GPP products as large observation-based vegetation productivity  
385 data sets. The flux tower-based GPP products (1982-2011) were provided by the Max Plank  
386 Institute for Biogeochemistry (MPI-BGC) with a spatial resolution of  $0.5^\circ \times 0.5^\circ$ , using the  
387 machine learning technique, model tree ensembles (MTE). FLUXNET observations of carbon  
388 dioxide, water and energy fluxes were upscaled with the trained MTE to generate global flux  
389 fields at a  $0.5^\circ \times 0.5^\circ$  spatial resolution and a monthly temporal resolution ([https://www.bgc-  
390 jena.mpg.de/geodb/projects/Home.php](https://www.bgc-jena.mpg.de/geodb/projects/Home.php)).

391 **Normalized Difference Vegetation Index and MODIS Enhanced Vegetation Index data:**  
392 We used the biweekly third generation of Normalized Difference Vegetation Index (NDVI3g;  
393 1982-2011) data obtained from the Global Inventory Modeling and Mapping Studies (GIMMS)  
394 group (available at <https://ecocast.arc.nasa.gov/data/pub/gimms/>), with a spatial resolution of  
395  $1/12$  degree ( $\sim 8$ km). The GIMMS-NDVI3g data generated from the calibrated Advanced Very  
396 High Resolution Radiometer (AVHRR) have been carefully corrected for sensor degradation,  
397 intersensor differences, cloud cover, solar zenith angle, viewing angle effects due to satellite  
398 drift and volcanic aerosols<sup>62,63</sup>. Here we investigated the long-term NDVI data, as a proxy of  
399 plant photosynthesis, to monitor the vegetation growth. We first composited the biweekly  
400 GIMMS-NDVI3g data to monthly temporal resolution by selecting the maximal one of the two  
401 composites in the same month, and then were aggregated to  $0.5^\circ \times 0.5^\circ$  to match the resolution

402 of GPP data and meteorological data.

403 Given that NDVI data might suffer from saturation (or cloud contaminations) in high  
404 biomass (or rainfall) regions, we also used monthly MODIS enhanced vegetation index (EVI)  
405 data (MOD13C2, Collection 6), optimizing the vegetation signal with reductions in  
406 atmospheric cloud and aerosol contaminations effects, as a complementary proxy to provide  
407 more confidence in interpreting peak vegetation growth. The monthly MODIS EVI data at 0.05°  
408 spatial resolution (2000-2011) were obtained from the online Data Pool at the NASA Land  
409 Processes Distributed Active Archive Centre, U.S. Geological Survey/Earth Resources  
410 Observation and Science Centre (<https://lpdaac.usgs.gov>). The algorithm uses the MODIS  
411 surface reflectance data in the blue, red and near-infrared spectral bands as its inputs to retrieve  
412 EVI data<sup>64</sup>. The gridded EVI data sets include pixel-level quality assurance (QA) flags as well  
413 as statistics of EVI quality and input data<sup>65</sup>. To get high-quality EVI composites, we filtered  
414 the original data based on the QA layer by selecting the pixels flagged as “good quality”. Gaps  
415 remaining after QA filtering were filled by interpolation in the temporal dimension, computing  
416 the values of gaps by fitting linearly between the two adjacent points. The time series with  
417 more than two consecutive gaps were excluded from further analyses. The data was then  
418 mosaicked and re-projected by using the MODIS Reprojection Tool, and mosaicked images  
419 resampled into 0.5° × 0.5° (latitude × longitude) resolution by using the nearest neighbor  
420 algorithm.

421 **Sun-induced chlorophyll fluorescence data:** We analyzed the sun-induced chlorophyll  
422 fluorescence (SIF) data to investigate vegetation photosynthetic capacity at the community-  
423 level. The SIF data was produced using spectra from the Global Ozone Monitoring  
424 Experiment-2 (GOME-2) instrument onboard the MetOp-A platform<sup>19</sup>. SIF retrievals were  
425 performed in the 715nm-758nm spectral window with ~0.5nm spectral resolution<sup>66</sup>. The SIF  
426 products used in this study were GOME2\_F level 3 monthly retrievals (2007-2015) with a  
427 spatial resolution of 0.5°×0.5° (<http://avdc.gsfc.nasa.gov/index.php>). The GOME-2 level 3 SIF  
428 retrievals have been quality-filtered, aggregated as monthly averages and gridded globally.  
429 Previous studies have reported that SIF could be a robust indicator of GPP, though the  
430 uncertainties existed in the GPP-SIF relationship<sup>19,67</sup>.

431 **Peak plant growth analysis:** MTE GPP<sub>max</sub>, GIMMS NDVI<sub>max</sub> and SIF<sub>max</sub> data were used as  
432 proxies of peak vegetation growth. Global gridded peak plant growth (GPP<sub>max</sub>, NDVI<sub>max</sub> and  
433 SIF<sub>max</sub>) datasets were compiled annually by picking out the maximal one from the monthly  
434 composites of the same year in each grid cell. In particular, the long-term MTE GPP<sub>max</sub> and  
435 NDVI<sub>max</sub> products were identified to monitor the linear trends of the global peak vegetation  
436 growth in the past three decades. The spatial pattern of linear trends in each dataset was  
437 calculated and evaluated using the Mann-Kendall test at the 5% significance level. Regions  
438 where trends were not statistically significant ( $P>0.05$ ) were set as missing values and labelled  
439 by blank ones in figures. All the data calculations were accomplished in R ([http://www.r-](http://www.r-project.org/)  
440 [project.org/](http://www.r-project.org/)).

441 **Forcing data sets:** Forcing data sets were involved to investigate the contribution of multiple  
442 factors to annual changes of NDVI<sub>max</sub> over 1982–2010, including radiation, air temperature,  
443 precipitation, fraction of cropland, nitrogen deposition and rising CO<sub>2</sub> concentration. Monthly  
444 climatology (including air temperature, precipitation) data with a spatial resolution of 0.5°×0.5°  
445 were obtained from meteorological data stored at the Climate Research Unit, University of East  
446 Anglia (CRU TS 3.23)<sup>68</sup>. We obtained 0.5°×0.5° gridded data of monthly downward shortwave  
447 radiation at surface (W m<sup>-2</sup>) from the Terrestrial Hydrology Research Group at Princeton  
448 University<sup>69</sup> (<http://hydrology.princeton.edu/data/pgf/v2/0.5deg/monthly/>). The annual global  
449 gridded (0.5°×0.5°) cropland fraction change data set (1982-2010) were obtained from Hurtt  
450 et al.<sup>70</sup> ([http://daac.ornl.gov/cgi-bin/dsvviewer.pl?ds\\_id=1248](http://daac.ornl.gov/cgi-bin/dsvviewer.pl?ds_id=1248)), and was used as the agriculture  
451 driving factor in analyzing the dominators of observed peak plant growth (NDVI<sub>max</sub>). Here the  
452 global gridded (0.5°×0.5°) atmospheric components changes data consisted of atmospheric  
453 nitrogen deposition and atmospheric CO<sub>2</sub> concentration ([CO<sub>2</sub>]) data. Both of the two data sets  
454 were obtained from the MsTMIP environmental driver data sets for the historical period<sup>36,71</sup>.  
455 The atmospheric [CO<sub>2</sub>] data prepared for the MsTMIP could be downloaded from ORNL  
456 DAAC at a monthly time scale, then averaged to annual mean to match the NDVI<sub>max</sub> data.  
457 Based on Dentener's maps and introduced spatio-temporal variation from nitrogen emissions<sup>72</sup>,  
458 the time-varying annual nitrogen deposition rate (NH<sub>x</sub>-N and NO<sub>y</sub>-N) data were used in this  
459 study.

460 **Relative importance calculation:** We used a relative importance analysis approach to quantify  
461 the relative contributions of each factor (i.e., radiation, air temperature, precipitation, fraction  
462 of cropland, nitrogen deposition and rising CO<sub>2</sub>) to the annual changes of NDVI<sub>max</sub> in each grid  
463 cell, expressed as the Pearson correlation in a multiple linear regression (NDVI<sub>max</sub> = b<sub>0</sub> +  
464 b<sub>1</sub>×Radiation + b<sub>2</sub>×Temperature + b<sub>3</sub>×Precipitation + b<sub>4</sub>×Cropland fraction + b<sub>5</sub>×NDE +  
465 b<sub>6</sub>×CO<sub>2</sub> + ε). ε represented other drivers that were not considered but might contribute to  
466 NDVI<sub>max</sub> variation. The algorithm was performed with the ‘relaimpo’ package in R (R  
467 Development Core Team 2011), which is based on variance decomposition for multiple linear  
468 regression models<sup>73</sup>. The ‘relaimpo’ package provides six different methods for analyzing  
469 relative importance of each regressor in linear regression. We chose one of the most computer-  
470 intensive and common-used method named ‘Lindeman-Merenda-Gold (LMG)’. The LMG  
471 method allows to differentiate the contribution of different correlated regressors in a multiple  
472 linear regression. The ‘LMG’ method estimated the relative importance (RI<sub>v</sub>) of each variable  
473 by splitting the total  $r^2$  into one non-negative  $r^2$  shared by per variable. In multiple regression  
474 models, the sequential  $r^2$  strongly depended on the order of the regressors. In other words, the  
475 sequential  $r^2$  derived from LMG was obtained by averaging all the possible orderings. Finally,  
476 all the RI<sub>v</sub> values were normalized (divided by  $r^2$ ) to sum to 1.

477 In each grid cell, we calculated the contributions of each factor to inter-annual NDVI<sub>max</sub>  
478 (Supplementary Fig. 4). Then the global attributions to NDVI<sub>max</sub> were calculated by averaging  
479 the values of contributors at the pixel-level (statistically significant pixels;  $P < 0.05$ ).

480 **In situ-observation data set:** In order to test whether crops have higher photosynthetic  
481 capacity than natural plant species, we investigated measured leaf-level maximum  
482 carboxylation rate ( $V_{cmax}$ ) and flux tower-observed GPP<sub>max</sub> at the ecosystem-level, which were  
483 analyzed using the probability density function. The leaf-level maximal carboxylation rate  
484 ( $V_{cmax}$ ,  $\mu\text{mol m}^{-2} \text{s}^{-1}$ ) data of 612 observations across 81 plant species were compiled from the  
485 TRY database<sup>15</sup> (<http://www.try-db.org>), a coverage of plant trait data representing the plant  
486 functional diversity on global scale. Leaf  $V_{cmax}$  data were then divided into crops, trees and  
487 grasses to explore the differences of probability density among species<sup>21-23</sup>. Photosynthetic  
488 capacity simulations within earth system models were closely associated with  $V_{cmax}$ <sup>45</sup>. The

489 measured multi-species leaf  $V_{\text{cmax}}$  in Fig. 3a indicated the overall difference in leaf-level plant  
490 photosynthetic capacity differences across crops, trees and grasses.

491 We also used eddy covariance flux data of GPP from 213 FLUXNET sites (including  
492 forest, grassland and cropland) of the La Thuile Database ([www.fluxdata.org](http://www.fluxdata.org)), a combination  
493 of measurements from the networks Ameriflux, CarboEurope and Fluxnet-Canada for the time  
494 period 1992-2006. According to the methods and criteria in Reichstein et al.<sup>74</sup> and Papale et  
495 al.<sup>75</sup>, data of each site-year in the database was filtered. Due to the inevitable data uncertainties  
496 arising from indirect measurement and some negative values in some site years, only site years  
497 with more than 300 daily estimates were chosen from the database. Comprehensive fit  
498 functions and algorithms were developed to derive the flux tower  $\text{GPP}_{\text{max}}$  of each site in  
499 different biomes. List of flux sites and details about the flux  $\text{GPP}_{\text{max}}$  calculation methods were  
500 described in Xia et al.<sup>1</sup>.

501 **Meta-analysis of leaf biomass data:** We conducted a systematic meta-analysis to further  
502 explain the higher contributions of atmospheric  $[\text{CO}_2]$  and nitrogen deposition relative to  
503 climate change on  $\text{NDVI}_{\text{max}}$ , according to the guidelines listed in the PRISMA (preferred  
504 reporting items for systematic reviews and meta-analyses) statement ([http://www.prisma-](http://www.prisma-statement.org/)  
505 [statement.org/](http://www.prisma-statement.org/)). We collected data from journal articles related to the response of terrestrial  
506 plant growth to changes of environmental factors ( $\text{CO}_2$ , nitrogen and temperature). We  
507 searched peer-reviewed and primary research papers from Web of Science, published before  
508 December 2016. Candidate papers were individually examined for data meeting the following  
509 criteria: (i) both control and treatment existed (ii) the responses were provided at species level,  
510 and the means ( $X$ ), sample sizes ( $n$ ), standard deviations ( $\text{SD}$ ) or standard errors ( $\text{SE}$ ) under the  
511 control and treatment were also provided; (iii) the examined responsive variables encompassed  
512 plant parts, i.e. whole, aboveground, belowground, leaf, root, stem, etc. Since the sample size  
513 and variance of the original studies were included in our data collections, our meta-analysis  
514 followed the guidelines set by Vetter et al.<sup>76</sup>. Based on these, a total of 466 studies under  
515 treatment (warming, nitrogen addition and elevated  $\text{CO}_2$ ) were collected to do further analysis  
516 (Supplementary Fig.6; Supplementary Table 2). The first dataset of plant growth response

517 under each treatment were then produced. Here we examined the response of leaf biomass from  
 518 466 manipulative experiments to warming, nitrogen addition, and elevated CO<sub>2</sub>, respectively.  
 519 Moreover, we separated the experimental data into different plant functional types (woody,  
 520 herb, tree, shrub, grass or forb) and climatic zones (tropical, temperate or boreal). Overall, there  
 521 were 92 observations (warming), 234 observations (nitrogen addition) and 113 observations  
 522 (elevated CO<sub>2</sub>) of leaf growth data in our meta-analysis.

523 For those studies which provided SE, SD was calculated by

$$524 \quad SD = SE\sqrt{n}, \quad (1)$$

525 The meta-analysis followed the techniques described in Hedge et al.<sup>77</sup>. The response of  
 526 leaf growth to treatments was estimated using the natural logarithm transformed response ratio  
 527 (RR):

$$528 \quad \ln RR = (X_C/X_T), \quad (2)$$

529 where  $X_C$  was the mean value of leaf biomass under the control treatment, and  $X_T$  denoted the  
 530 mean value of corresponding treatment (warming, nitrogen addition or elevated CO<sub>2</sub>). The  
 531 variance of the  $\ln (RR)$  was:

$$532 \quad v = \left( \frac{SD_C^2}{n_C X_C^2} + \frac{SD_T^2}{n_T X_T^2} \right), \quad (3)$$

533 where  $SD_C$  and  $SD_E$  were the standard deviation of  $X_C$  and  $X_T$ , and  $n_C$  and  $n_T$  represented the  
 534 sample sizes of  $X_C$  and  $X_T$ , respectively.

535 After the multiplied groups of natural log-transformed response ratio reflecting each effect  
 536 (warming, nitrogen deposition and elevated CO<sub>2</sub>) were calculated, the random-effects model  
 537 was used to get the weighted mean. Then the weighted response ratio (RR<sub>++</sub>) is calculated as  
 538 below (m is the number of groups, k is the number of comparison):

$$539 \quad RR_{++} = \frac{\sum_{i=1}^m \sum_{j=1}^k W_{ij} RR_{ij}}{\sum_{i=1}^m \sum_{j=1}^k W_{ij}} \quad (4)$$

540 and its standard error were calculated as below:

$$541 \quad S (RR_{++}) = \sqrt{\frac{1}{\sum_{i=1}^m \sum_{j=1}^k W_{ij}}} \quad (5)$$

542 Then the 95% confidence interval (95% CI) was  $RR_{++} \pm 1.96 \times S (RR_{++})$ , and was  
543 generated by bootstrapping the data using Metawin 2.1 (Sinauer Associates Inc., Sunderland,  
544 MA, USA). The results were back-transformed and represented as percentage change by  $(exp$   
545  $(RR_{++} - 1)) \times 100 \%$ . The response was considered significant if the 95% CI did not overlap with  
546 zero.

547 **Processing model outputs from MsTMIP:** To further evaluate the simulated global peak  
548 vegetation growth trends and their driving factors,  $GPP_{max}$  of fifteen MsTMIP models were  
549 used during 1982–2010. The models were forced with consistent driver datasets, and the  
550 simulation protocol and details of the forcing data have been described in Huntzinger et al.<sup>20</sup>  
551 and Wei et al.<sup>36</sup>. We performed a series of experimental simulations to analyze the four main  
552 drivers (i.e., climate change, land cover and land use change, CO<sub>2</sub> fertilization and nitrogen  
553 deposition) of simulated global vegetation growth peak: initial condition with all  
554 environmental drivers constant (RG1); varying climate (temperature, precipitation and  
555 radiation) only (SG1); varying climate and land cover and land use (SG2); varying climate,  
556 land cover and land use, and CO<sub>2</sub> (SG3); and (BG1) varying climate and land cover and land  
557 use, CO<sub>2</sub> and nitrogen deposition. Simulations SG1-RG1, SG2-SG1, SG3-SG2 and BG1-SG3  
558 were used to evaluate the effects of climate change, LULCC, CO<sub>2</sub> fertilization, and nitrogen  
559 deposition to vegetation growth peak, respectively. Currently, it should be noted that not all  
560 fifteen models submitted all the four sensitivity simulations, especially for the nitrogen  
561 deposition (Supplementary Table 1). Thus, we conducted the factorial experiments in two sub-  
562 ensembles: 8 models with nitrogen limitation (+ Nitrogen) and 7 models without nitrogen  
563 limitation (- Nitrogen), respectively. An attribution analysis for each individual model in the  
564 sub-ensembles was completed and then values were averaged across the models. Additionally,  
565 current model Intercomparison projects (MIPs) consider the climate change scenario (SG1) as  
566 a combination of temperature, precipitation and radiation, making direct comparison with the  
567 relative importance calculations less comprehensive. We recommend that future MIPs request  
568 outputs from model simulations under separated climate factor scenario to allow for more direct  
569 comparisons with observation-based attributions. We also request a possible scenario as a  
570 combination of varying climate and varying CO<sub>2</sub> to attribute the LULCC effect in the future

571 model inter-comparison experiments.

572 **Carbon use efficiency data set:** The carbon use efficiency (CUE) was calculated as the ratio  
573 of net primary productivity (NPP) to GPP. Both in-situ GPP and NPP data were obtained from  
574 the database in DeLucia et al.<sup>78</sup>, Campioli et al.<sup>79</sup> and Chen et al.<sup>80</sup>. Here we presented a CUE  
575 data set of 139 site-years (Supplementary Fig.15) comprising forests, grasslands and croplands.  
576 According to the management status and treatments, sites were divided into natural, elevated  
577 CO<sub>2</sub> and fertilized.

578 **Code availability.** The code used to generate the results shown can be obtained from the  
579 corresponding author upon request.

580 **Data availability.** The authors declare that the data supporting the finding of this study are  
581 available within the article and its Supplementary Information files.

## 582 **References**

- 583 62. Piao, S. *et al.* Evidence for a weakening relationship between interannual temperature  
584 variability and northern vegetation activity. *Nat. Commun.* **5**, 5018 (2014).
- 585 63. Tucker, C. J. *et al.* An extended AVHRR 8 - km NDVI dataset compatible with MODIS  
586 and SPOT vegetation NDVI data. *Int. J. Remote Sens.* **26**, 4485-4498 (2005).
- 587 64. Huete, A. *et al.* Overview of the radiometric and biophysical performance of the  
588 MODIS vegetation indices. *Remote Sens. Environ.* **83**, 195-213 (2002).
- 589 65. Zhou, L. *et al.* Widespread decline of Congo rainforest greenness in the past decade.  
590 *Nature* **509**, 86-90 (2014).
- 591 66. Joiner, J. *et al.* Global monitoring of terrestrial chlorophyll fluorescence from moderate-  
592 spectral-resolution near-infrared satellite measurements: methodology, simulations,  
593 and application to GOME-2. *Atmos. Meas. Tech.* **6**, 2803-2823 (2013).
- 594 67. Parazoo, N. C. *et al.* Interpreting seasonal changes in the carbon balance of southern  
595 Amazonia using measurements of XCO<sub>2</sub> and chlorophyll fluorescence from GOSAT.  
596 *Geophys. Res. Lett.* **40**, 2829-2833 (2013).

- 597 68. Harris, I., Jones P. D., Osborn T. J. & Lister D. H. Updated high-resolution grids of  
598 monthly climatic observations – the CRU TS3.10 Dataset. *Int. J. Climatol.* **34**, 623-642  
599 (2014).
- 600 69. Sheffield, J., Goteti, G. & Wood, E. F. Development of a 50-year high-resolution global  
601 dataset of meteorological forcings for land surface modeling. *J. Clim.* **19**, 3088-3111  
602 (2006).
- 603 70. Hurtt, G. C. *et al.* Harmonization of land-use scenarios for the period 1500–2100:  
604 600 years of global gridded annual land-use transitions, wood harvest, and resulting  
605 secondary lands. *Climatic Change* **109**, 117-161 (2011).
- 606 71. Wei, Y. *et al.* NACP MsTMIP: Global and North American Driver Data for Multi-  
607 Model Intercomparison. ORNL DAAC, Oak Ridge, Tennessee, USA.  
608 <http://doi.org/10.3334/ORNLDAAC/1220> (2014).
- 609 72. Dentener, F. J. Global Maps of Atmospheric Nitrogen Deposition, 1860, 1993, and 2050.  
610 Data Set. Oak Ridge National Laboratory Distributed Active Archive Center, Oak  
611 Ridge, Tennessee, USA. Available at: <http://daac.ornl.gov> (2006).
- 612 73. Grömping, U. Relative importance for linear regression in R: the package relaimpo.  
613 *Journal of statistical software* **17**, 1-27 (2006).
- 614 74. Reichstein, M. *et al.* On the separation of net ecosystem exchange into assimilation and  
615 ecosystem respiration: review and improved algorithm. *Glob. Change Biol.* **11**, 1424-  
616 1439 (2005).
- 617 75. Papale, D. *et al.* Towards a standardized processing of Net Ecosystem Exchange  
618 measured with eddy covariance technique: algorithms and uncertainty estimation.  
619 *Biogeosciences* **3**, 571-583 (2006).
- 620 76. Vetter, D., Rücker, G., Storch, I. Meta-analysis: A need for well-defined usage in  
621 ecology and conservation biology. *Ecosphere* **4**, 1-24 (2013).
- 622 77. Hedges, L. V., Gurevitch, J. & Curtis, P. S. The meta-analysis of response ratios in  
623 experimental ecology. *Ecology* **80**, 1150-1156 (1999).
- 624 78. DeLucia, E. H., Drake, J. E., Thomas, R. B. & Gonzalez-Meler, M. Forest carbon use  
625 efficiency: Is respiration a constant fraction of gross primary production? *Glob. Change*  
626 *Biol.* **13**, 1157-1167 (2007).

- 627 79. Campioli, M. *et al.* Biomass production efficiency controlled by management in  
628 temperate and boreal ecosystems. *Nat. Geosci.* **8**, 843-846 (2015).
- 629 80. Chen, Z., Yu, G., Wang, Q. Ecosystem carbon use efficiency in China: Variation and  
630 influence factors. *Ecol. Indic.* **90**, 316-323 (2018).

### 631 **Acknowledgements**

632 We wish to thank the four anonymous reviewers for their valuable suggestions on the  
633 manuscript. This work was financially supported by the National Key R&D Program of China  
634 (2017YFA0604600), the National Natural Science Foundation (31430015, 41601099,  
635 41630528), and the National 1000 Young Talents Program of China. We thank all the people  
636 and institutions that worked to provide data for this study, particularly the MsTMIP modeling  
637 group. We also thank the MTE GPP products provided by MPI-BGC (Max Planck Institute for  
638 Biogeochemistry, Jena, Germany), biweekly NDVI data from the GIMMS team, MODIS EVI  
639 products provided by USGS, climate forcing data from CRU and Princeton University, CO<sub>2</sub>  
640 site data from NOAA, and Eumetsat for the GOME-2 SIF retrievals. We further thank the TRY  
641 initiative for plant traits (<http://www.try-db.org>). The TRY initiative and database is hosted,  
642 developed and maintained by J. Kattge and G. Bönisch (MPI-BGC). The eddy-covariance data  
643 of La Thuile FLUXNET used in this study were mainly acquired by the following networks:  
644 AmeriFlux, GHG-Europe, SOERE, FORE-T, Fluxnet-Canada Research Network (supported  
645 by CFCAS, NSERC, BIOCAP, Environment Canada, and NRCan), GreenGrass, KoFlux, LBA,  
646 NECC, OzFlux, TCOS-Siberia and USCCC. Author J.B.F. contributed to this paper from the  
647 Jet Propulsion Laboratory, California Institute of Technology, under a contract with the  
648 National Aeronautics and Space Administration; and support was provided by the INCA  
649 program.

### 650 **Author contributions**

651 J.Xia designed the study. K.Huang performed the analysis. J.X. and K.H. wrote the first draft.  
652 Y.L., Y.W., A.A., J.C., E.C., Z.L., Q.Y., X.X. and L.Y. contributed to the idea development.  
653 C.S., D.N.H., R.C., Y.F., J.B.F., A.M.M., K.S., Y.W. provided the modeling results. All authors

654 interpreted the results and revised the manuscript.

655 **Competing financial interests**

656 The authors declare no competing financial interests.

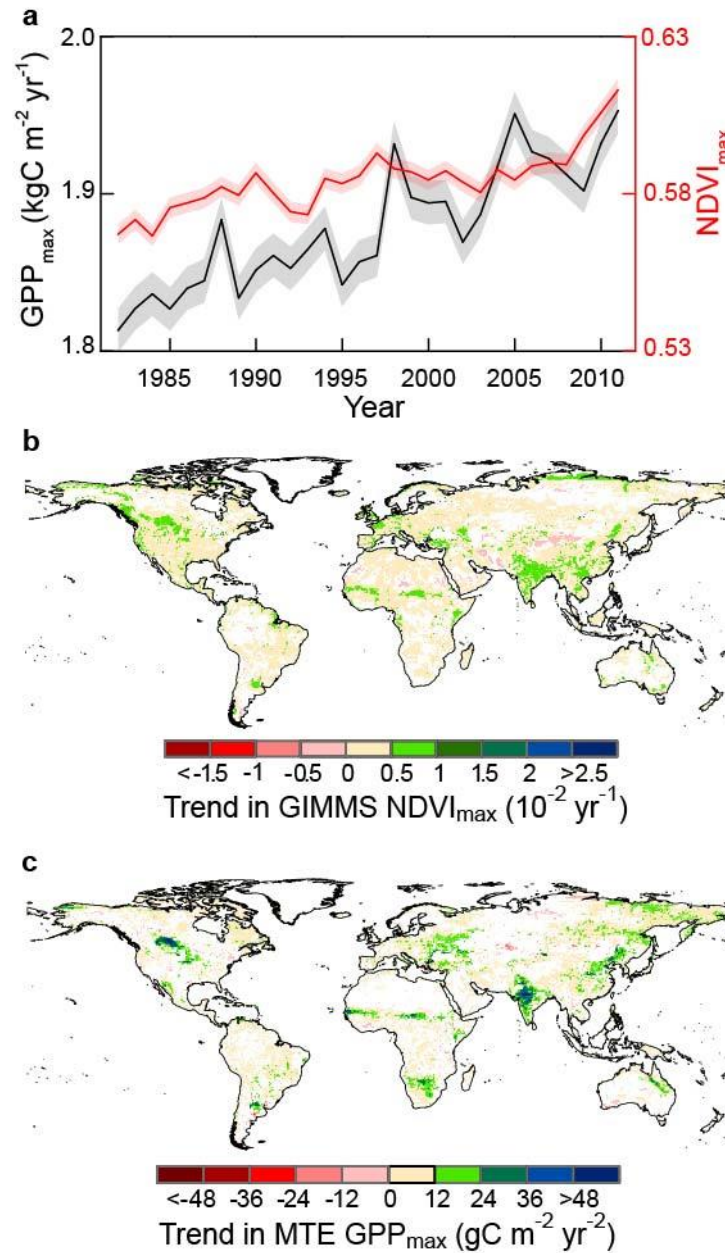
657

658 **Tables**

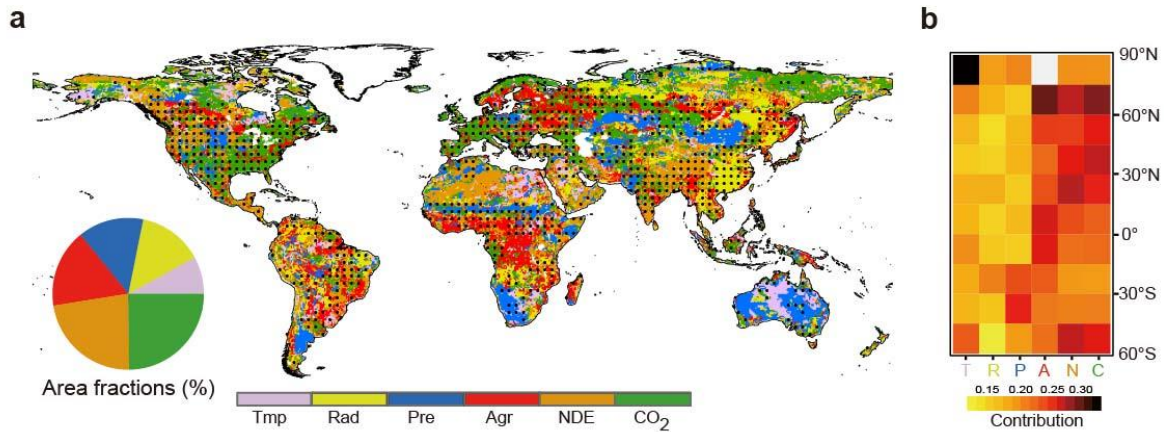
659 **Table 1** | Summary of response of global GPP<sub>max</sub> trend (g C m<sup>-2</sup> yr<sup>-2</sup>) modeled by multi-model  
 660 ensemble mean (MMEM) to climate change (CLI), land use and land cover change (LULCC),  
 661 rising CO<sub>2</sub> (CO<sub>2</sub>) and nitrogen deposition (NDE). Trends are statistically significant (Mann-  
 662 Kendall test;  $P < 0.05$ ).

Model	CLI	LULCC	CO <sub>2</sub>	NDE	N cycle
CLASS-CTEM-N	9.90	-1.52	17.71	-3.89	yes
CLM4	4.12	0.84	2.05	1.16	yes
CLM4VIC	3.95	0.17	1.88	1.30	yes
DLEM	3.77	0.08	3.41	1.26	yes
GTEC	2.14	3.32	4.75	/	no
ISAM	-1.34	-0.58	7.03	0.01	yes
LPJ-wsl	7.57	-0.68	7.91	/	no
ORCHIDEE-LSCE	3.80	1.91	6.98	/	no
SiB3-JPL	3.10	0.72	4.63	/	no
SiB3CASA	2.78	0.29	7.45	/	no
TEM6	5.30	-2.72	4.57	0.86	yes
VEGAS2.1	5.21	0.24	1.31	/	no
VISIT	3.38	0.20	8.20	/	no
BIOME-BGC	2.71	/	/	/	yes
TRIPLEX-GHG	/	/	6.77	0.08	yes

663

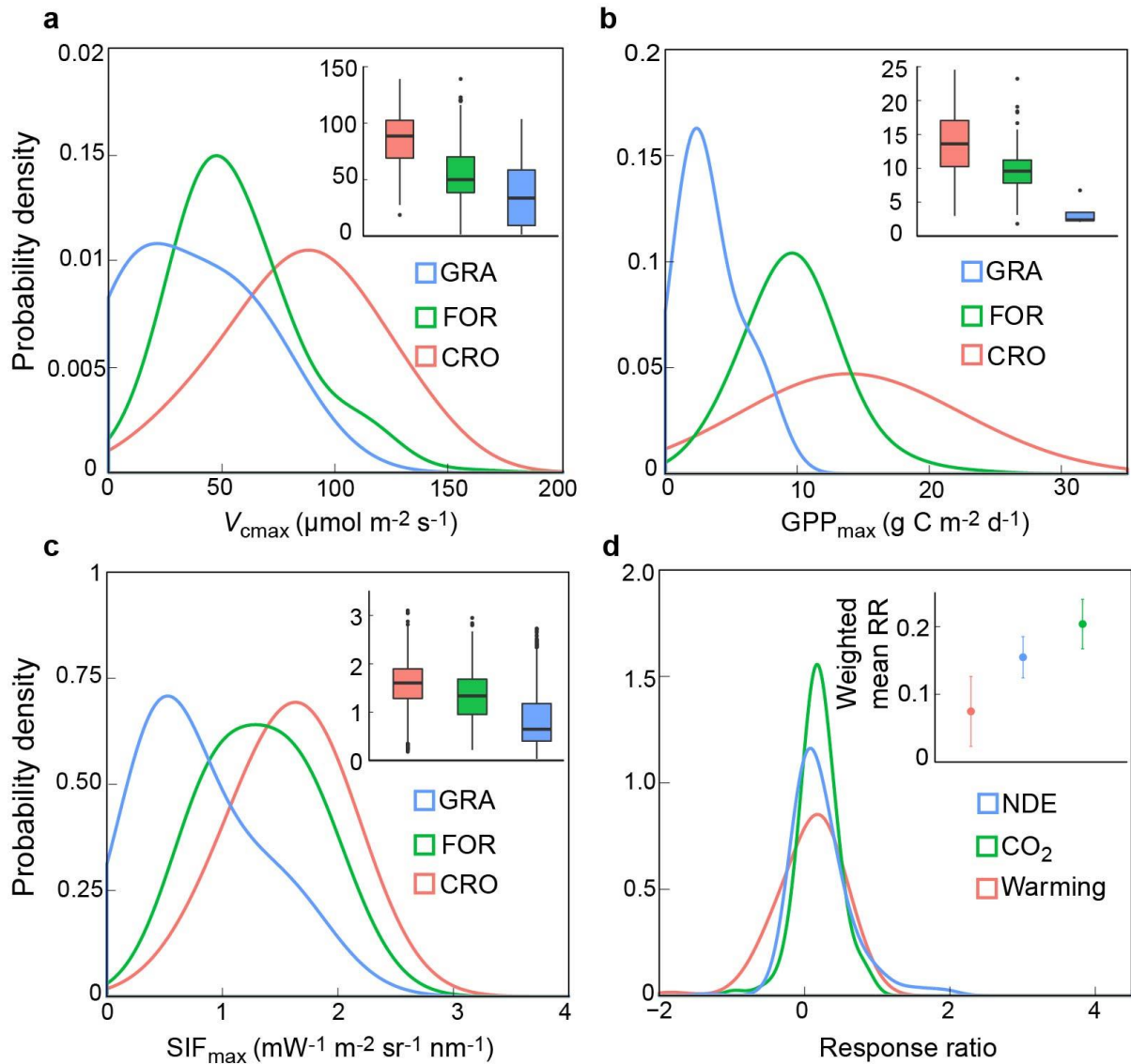


665  
 666 **Fig. 1 | Enhanced monthly vegetation-growth peak.** **a**, Annual time series of annual MTE  
 667 GPP<sub>max</sub> (black line) and GIMMS NDVI<sub>max</sub> (red line) over 1982–2011. The shaded areas  
 668 represent one standard error (SE). **b**, **c**, Spatial pattern of the trend in annual GIMMS NDVI<sub>max</sub>  
 669 in **b** and MTE GPP<sub>max</sub> in **c**, with white indicating those areas with no significant changes  
 670 ( $P > 0.05$ ). The  $P$ -values are calculated with the Mann-Kendall test.



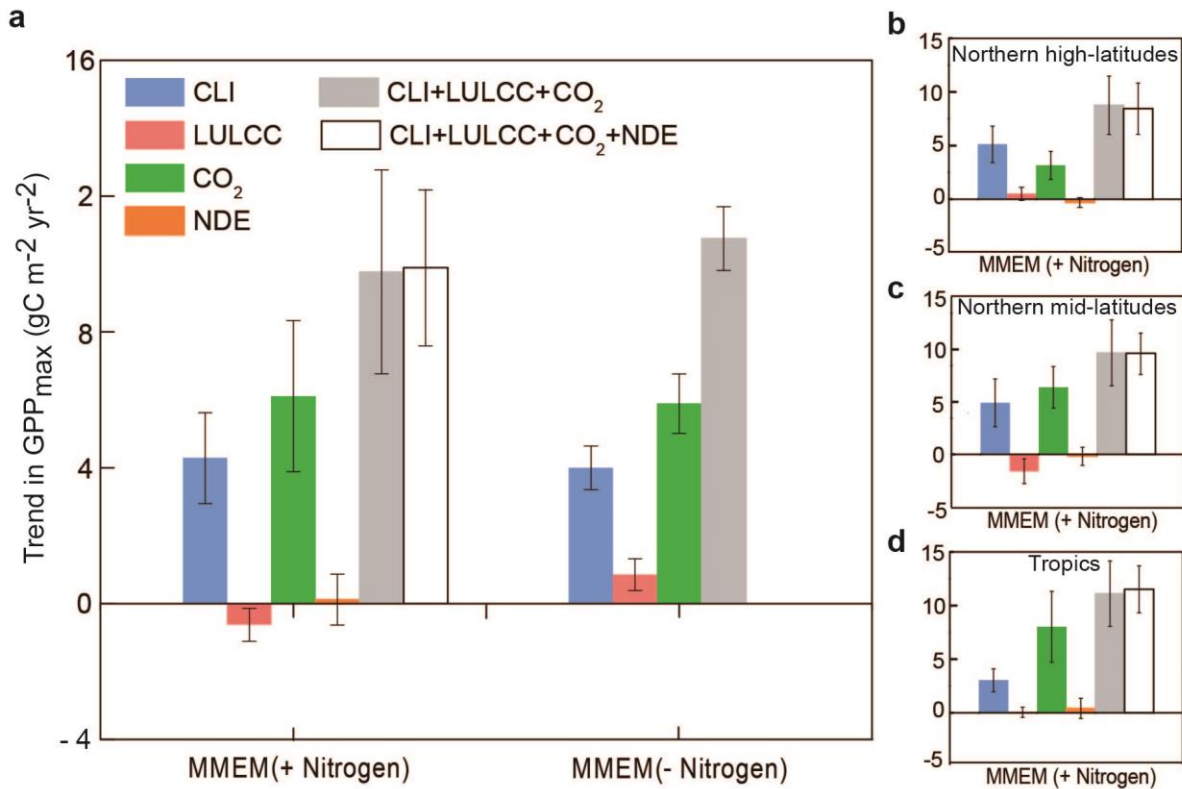
671

672 **Fig. 2 | Attribution of monthly vegetation-growth peak (NDVI<sub>max</sub>).** a, Dominant factors of  
 673 trends in NDVI<sub>max</sub>, defined as the driving factor that contributes the most to the increase (or  
 674 decrease) in NDVI<sub>max</sub> in each grid cell. The regions that are statistically significant ( $P < 0.05$ )  
 675 are labeled with black dots. The six driving factors include incoming shortwave radiation (Rad),  
 676 monthly average air temperature (Tmp), monthly precipitation (Pre), annual agriculture  
 677 cropland fractional changes (Agr), nitrogen deposition (NDE), and rising CO<sub>2</sub> (CO<sub>2</sub>). Inset: Pie  
 678 chart showing the area fractions of lands dominated by each attributor. b, Contributions of six  
 679 driving factors in 15° latitude bands (90°N-60°S). The six driving factors contributed to  
 680 NDVI<sub>max</sub> include Tmp (T), Rad (R), Pre (P), Agr (A), NDE (N), and CO<sub>2</sub>(C).



681

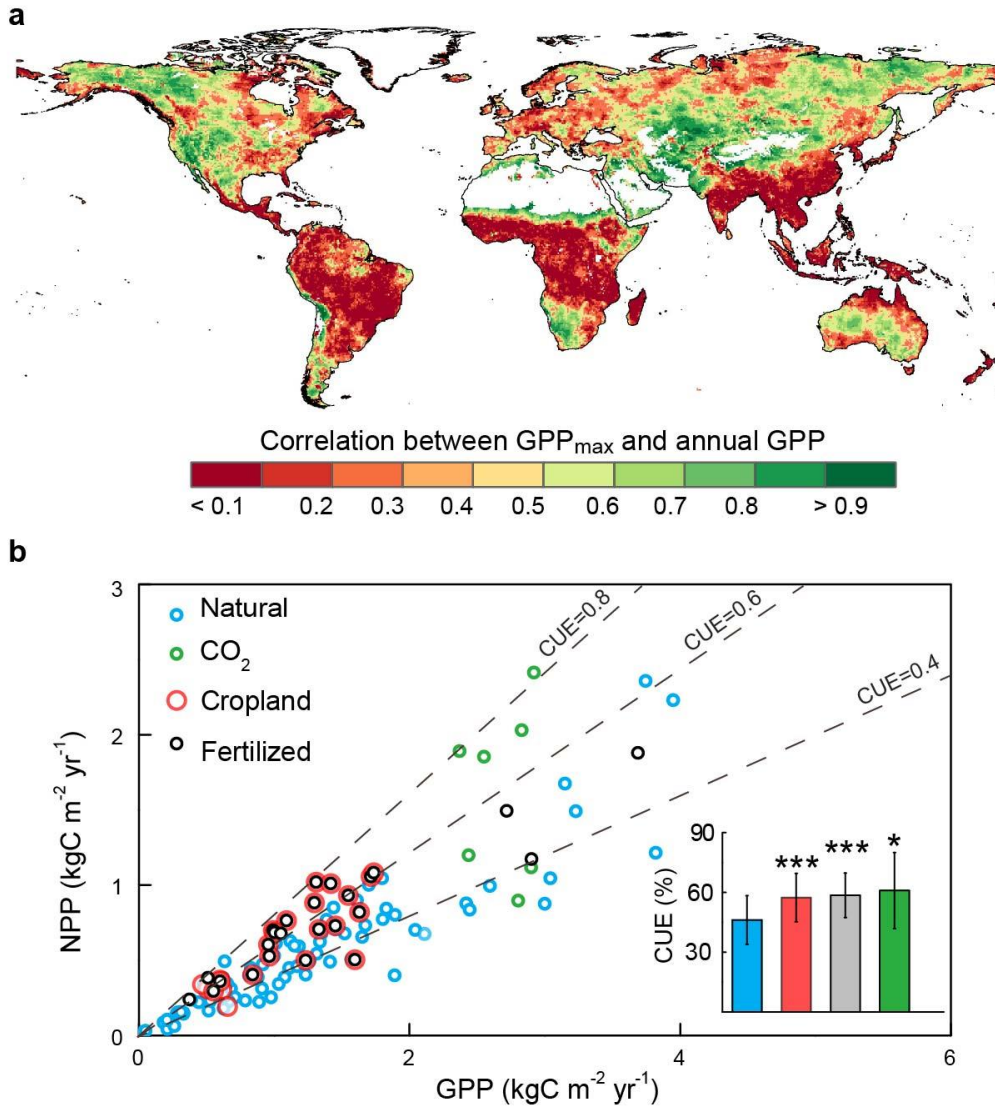
682 **Fig. 3 | Higher photosynthetic capacity of croplands.** The probability density function (PDF)  
 683 of three data set are calculated for cropland (CRO), forest (FOR), and grassland (GRA)  
 684 ecosystems. Probability density distributions of photosynthesis capacity by leaf-level  $V_{cmax}$   
 685 from TRY database for each biome type are illustrated in **a**, ecosystem-level flux tower-based  
 686 seasonal  $GPP_{max}$  across the FLUXNET sites in **b** and community-level  $SIF_{max}$  over 2007–2015  
 687 derived from GOME-2 in **c**. The inset boxplots in **a-c** indicate 25% and 75% percentiles.  
 688 Median values are shown by black horizontal bars in each box. **d** shows the PDF of natural  
 689 logarithm transformed leaf biomass response ratio (RR) to nitrogen addition, elevated  $\text{CO}_2$ ,  
 690 and warming treatments. Inset in **d** shows the weighted mean RR  $\pm$  95% confident intervals  
 691 (CIs) of leaf biomass RR to the treatments using meta-analysis.



692

693 **Fig. 4 | Attribution of peak GPP trends using factorial simulations for ensemble mean of**  
 694 **models with (+ Nitrogen) and without (- Nitrogen) a coupled carbon-nitrogen cycle. a-d,**  
 695 **Attributions of modeled GPP<sub>max</sub> trends (g C m<sup>-2</sup> yr<sup>-2</sup>) over the globe (a), northern high-latitudes**  
 696 **(60~90°N; b), northern mid-latitudes (30~60°N; c), and tropics (0~30°N; d). Modelled trends**  
 697 **in monthly GPP<sub>max</sub> are estimated by multi-model ensemble mean (MMEM) from the Multi-**  
 698 **scale Terrestrial Model Intercomparison Project (MsTMIP) by land use and land cover change**  
 699 **(LULCC), nitrogen deposition (NDE), climate change (CLI), and rising CO<sub>2</sub> (CO<sub>2</sub>) using the**  
 700 **Mann-Kendall test ( $P < 0.05$ ) (see Methods). The MMEM is calculated in two sub-ensembles:**  
 701 **models with nitrogen limitation (+ Nitrogen) and models without nitrogen limitations (-**  
 702 **Nitrogen). Error bars show the standard error of GPP<sub>max</sub> trends derived from model simulations.**

703



704

705 **Fig. 5 | Correlation of MTE  $GPP_{max}$  with annual GPP and relationship between measured**

706 **NPP and GPP.** Panel **a** shows the global distribution of the  $r^2$  values between monthly MTE

707  $GPP_{max}$  and annual GPP over 1982-2011. Panel **b** shows the carbon use efficiency (CUE; the

708 NPP/GPP ratio) across multi-sites comprising forests, grassland and croplands according to the

709 management status: natural (unmanaged), elevated  $CO_2$  and fertilized (see Methods). Inset in

710 **b** shows higher CUE of managed sites than natural sites. One asterisk indicates statistically

711 significant difference between the managed and natural ( $P < 0.05$ ), and three asterisks indicate

712 significant difference at  $P < 0.001$ . The error bar denotes the one standard deviation ( $\pm$  SD) of

713 the CUE.